Biomolecular motion characterization by a self-distribution-function procedure in elastic incoherent neutron scattering

Salvatore Magazù,[1,][*] Giacomo Maisano,[1] Federica Migliardo,[1,2] and Antonio Benedetto[1]

[1]*Dipartimento di Fisica, Università di Messina, C. da Papardo n° 31, P.O. Box 55, Vill. S. Agata, 98166 Messina, Italy*

[2]*Laboratoire de Dynamique et Structure des Matériaux Moléculaires, UNESCO-L'Oreal University of Lille I, UMR CNRS 8024, 59655 Villeneuve d'Ascq Cedex, France*

In the present paper we first focus on the role of the instrumental resolution in elastic incoherent neutron scattering (EINS) where the connection between the self-distribution function (SDF) and the measured EINS intensity profile is highlighted. Second we show how the SDF procedure, previously introduced, allows both the total and the partial mean-square displacement evaluations through the total and the partial SDFs. Finally, we compare the SDF and the Gaussian procedures, by applying the two approaches to EINS data collected, by the IN13 backscattering spectrometer (Institute Laue-Langevin, Grenoble), on aqueous mixtures of two homologous disaccharides, i.e., sucrose and trehalose, and on myoglobin.

I. INTRODUCTION

It is well known that the characterization of the different molecular processes involved in the dynamics of some molecular and macromolecular systems of biophysical interest, such as, for example, bioprotectant-water mixtures, pure and hydrated polymeric systems, and hydrated and crystalline proteins, can be effectively investigated by evaluating the mean-square displacement (MSD) [1] from elastic incoherent neutron-scattering (EINS) data collected by varying temperature, energy resolution, wave vector, and energy range and by using isotopic labeling. More specifically, a wide temperature range can facilitate the spectral separation of different molecular processes according to their time scale, while the temperature dependence of the measured elastic intensity can provide information about the involved activation energies and, thus, the local potentials. On the other hand, a wide Q range (e.g., such as that of IN13 backscattering spectrometer at the Institute Laue-Langevin (ILL) in Grenoble with a Q range extending up to 5 Å^{-1}) can allow us to achieve a molecular assignment based on spatial features. Furthermore the use of proper energy window and energy resolution can allow us to identify specific molecular motions and, as shown by Doster *et al.* [2–4] with the so-called "elastic resolution spectroscopy," can allow us to derive the intermediate scattering function in the time domain from experiments performed with a different energy resolution. Finally the isotopic substitution, highlighting the contributions from specific system constituents, can allow us to identify specific motions.

In the framework of the Gaussian approach the MSD can be obtained by a linear regression in the Guinier plot (where the logarithm of the elastic intensity is plotted as a function of Q^2) for a set of points close to $Q=0$. However this approach does not allow us to separate the different contributions related to a specific spatial domain and furnishes MSD values which are dependent on the Q range used for the MSD evaluation.

The aim of the present work is to clarify various aspects of the self-distribution-function (SDF) procedure proposed in a previous work [5] for evaluating the total and the partial MSDs and to discuss the role of the instrumental resolution function in extracting the MSD. On that score we apply the procedure to EINS data collected by using the IN13 spectrometer at ILL on aqueous mixtures of two homologous disaccharides (i.e., sucrose and trehalose) and on dry myoglobin in trehalose environment.

Hydrated disaccharides are nowadays the object of intense research efforts motivated both by fundamental research and by their biotechnological applications. In particular, among disaccharides, trehalose has received a growing attention because of both its wide role in nature and its potential use as a highly efficient natural bioprotectant system. Trehalose and sucrose aqueous mixtures have been characterized by light scattering, e.g., photon correlation spectroscopy and Raman scattering, by neutron scattering, i.e., neutron diffraction, inelastic scattering and quasielastic neutron scattering (QENS), and by simulation studies [6–10]. These techniques pointed out that trehalose shows a higher solute-solvent interaction strength, a higher kosmotropic character, and a higher capability of dynamics switching off than sucrose.

Myoglobin stands out as the first structurally determined protein and has been the subject of many detailed studies by a large number of experimental and computational methods [11–16]. Cordone *et al.* [17,18] showed that the mean-square displacements and the density of state function are those of a harmonic solid up to room temperature and that the amplitude of the nonharmonic motions stemming from the interconversion among the protein's conformational substates is reduced with respect to the H_2O-solvated system, while their onset is shifted toward higher temperature.

It is well known that the scattering law $S(Q,\omega)$ is connected, in Planck's units, through its time Fourier transform

*Corresponding author; FAX: +39 090395004; smagazu@unime.it

(F_t), to the intermediate scattering function $I(Q,t)$ and, through its space-time Fourier transform $(F_{r,t})$, to the time-dependent spatial correlation functions $G(r,t)$ [19,20]. The scattering law $S(Q,\omega)$ is proportional to the observed neutron intensity, with the proportionality factors being represented by the incident and outgoing neutron wave vectors, the number of scattered atoms, and the scattering cross sections [e.g., $\sigma_{inc}(\text{hydrogen}) = 81,0$ barn and $\sigma_{inc}(\text{deuterium}) = 2,2$ barn]. For samples with mainly incoherent scattering cross sections, the relevant correlation function is the SDF $G_s(r,t)$ which, following Van Hove [21], represents the probability to find the same particle at distance r after a time t.

To overcome the difficulty to collect QENS spectra with a relatively great amount of material [22–24], Doster *et al.* [2–4] proposed an elegant way to get dynamical information by EINS measurements at different resolution values, so taking advantage from the fact that the elastic contribution is at low-energy transfer often a factor of 100–1000 higher than the quasielastic one.

In this framework, due to the energy instrumental resolution $\Delta\omega$, the experimentally accessible quantity is the scattering function $S_R(Q,\omega,\Delta\omega)$, i.e., the convolution of the scattering law with the instrumental resolution function $R(\omega,\Delta\omega)$ [19,20]. Now, if the resolution in the ω space is the Dirac delta function, its time Fourier transform, i.e., the resolution function in t space $R(t)$, is a constant with an infinite resolution time $\tau_{RES} = \infty$, with this being the case of elastic neutron scattering.

The opposite case is furnished by total neutron scattering which is characterized by a constant resolution function in the ω space; in this latter case, its time Fourier transform $R(t)$ is a Dirac delta function that, consequently, has a resolution time equal to zero, i.e., $\tau_{RES} = 0$. A resolution function with a nonzero but finite characteristic time gives rise to an elastic contribution to which all the motions with a characteristic time τ longer than the resolution time τ_{RES} contribute. On this concern, Doster *et al.* has showed that the measured EINS intensity profile function can be interpreted as the intermediate scattering function $I(Q,t_R)$ calculated at the instrumental resolution time t_R, $t_R = \frac{1}{\Delta\omega}$.

II. EXPERIMENTAL SECTION

Experimental data were collected by the IN13 spectrometer at ILL which is characterized by a relatively high energy of the incident neutrons (16 meV). The experimental set up

was incident wavelength of 2.23 Å, Q range of 0.28–4.27 Å^{-1}, and elastic energy resolution [full width at half maximum (FWHM)] of 8 μeV. Raw data were corrected for cell scattering and detector response and normalized to unity at $Q = 0.28$ Å^{-1}. Measurements were performed in the temperature range of 20–310 K on hydrogenated trehalose and sucrose in H$_2$O, purchased by Sigma-Aldrich, at a weight fraction value corresponding to 19 water molecules for each disaccharide molecule.

Trehalose and sucrose have the same chemical formula ($C_{12}H_{22}O_{11}$; $M_w = 342.3$), but different structures which could account for the different effectiveness. More precisely sucrose (α-D-glucopyranosil β-D-fructofuranoside) is constituted by a glucose ring (pyranose) in the α configuration and fructose ring (furanose) in the β configuration; the α and β structures of the same monosaccharide differ only in the orientation of the OH groups at same carbon atom in the ring itself (mutarotation equilibria). Trehalose (α-D-glucopyranosil β-D-fructofuranoside) is constituted by two pyranose (six-membered) rings in the same α configuration, linked by a glycosidic bond between the chiral carbon atoms C1 of the two rings. Both pure sugars form glasses at temperatures above ambient temperature, but the glass transition temperature T_g of sucrose is significantly lower than that of trehalose ($T_g^{sucrose} = 350$ K and $T_g^{trehalose} = 388$ K).

Myoglobin [11] is a small helical protein, closely related to hemoglobin, having the role of intracellular oxygen storage site and consisting of four myoglobinlike subunits that form a tetramer and are responsible for carrying oxygen in blood. Myoglobin data were taken from Refs. [2–4].

III. RESOLUTION EFFECTS

The scattering law $S(Q,\omega)$, linked to the intermediate scattering function $I(Q,t)$ by a time Fourier transform [11,12]

$$S(Q,\omega) = \frac{1}{\sqrt{2\pi}} \int_{-\infty}^{\infty} I(Q,t) e^{-i\omega t} dt \qquad (1)$$

becomes, at $\omega = 0$,

$$S(Q,\omega = 0) = \frac{1}{\sqrt{2\pi}} \int_{-\infty}^{\infty} I(Q,t) dt. \qquad (2)$$

Taking into account Eq. (1), the convolution of the scattering law with the instrumental resolution function results is

$$\begin{aligned}
S_R(Q,\omega;\Delta\omega) &= \left[\frac{1}{\sqrt{2\pi}} \int_{-\infty}^{\infty} I(Q,t) e^{-i\omega t} dt \right] \otimes R(\omega;\Delta\omega) = \int_{-\infty}^{+\infty} \frac{1}{\sqrt{2\pi}} \int_{-\infty}^{\infty} I(Q,t) e^{-i(\omega-\omega')t} dt \, R(\omega';\Delta\omega) d\omega' \\
&= \int_{-\infty}^{\infty} I(Q,t) e^{-i\omega t} dt \left[\frac{1}{\sqrt{2\pi}} \int_{-\infty}^{+\infty} e^{i\omega' t} R(\omega';\Delta\omega) d\omega' \right] = \int_{-\infty}^{\infty} I(Q,t) R(t) e^{-i\omega t} dt.
\end{aligned} \qquad (3)$$

Therefore the measured elastic contribution to the scattering is

$$S_R(Q, \omega = 0; \Delta\omega) = \int_{-\infty}^{\infty} I(Q, t) R(t) dt. \qquad (4)$$

In the ideal elastic case in which the resolution is a delta function in the ω space, we obtain that the measured scattering function is the scattering law evaluated at $\omega = 0$, i.e.,

$$S_R(Q, \omega = 0; \Delta\omega) = \int_{-\infty}^{\infty} I(Q, t) R(t) dt = \frac{1}{\sqrt{2\pi}} \int_{-\infty}^{\infty} I(Q, t) dt$$

$$= S(Q, \omega = 0). \qquad (5)$$

In the opposite limit in which the instrumental resolution is a very broad function in the ω space [with respect to the time behavior of $I(Q, t)$], under the assumption that it can be treated as a constant, the measured quantity corresponds to the intermediate scattering function evaluated at $t = 0$, i.e.,

$$S_R(Q, \omega = 0; \Delta\omega) = \int_{-\infty}^{\infty} I(Q, t) R(t) dt = \int_{-\infty}^{\infty} I(Q, t) \delta(t) dt$$

$$= I(Q, t = 0). \qquad (6)$$

For the general case evaluation, one can assume for the resolution in the ω space a Gaussian function, characterized by a resolution time τ_{RES}:

$$R(\omega; \tau_{\mathrm{RES}}) = C e^{-\omega^2 \tau_{\mathrm{RES}}^2 / 2}, \qquad (7)$$

where $C = a\left(\frac{1 + \tau_{\mathrm{RES}}}{\sqrt{2\pi}}\right)$ in order to guarantee the above discussed limit behaviors for $\tau_{\mathrm{RES}} \gg \tau$ and $\tau_{\mathrm{RES}} \ll \tau$. Furthermore, since the main focus here is not to derive specific time-dependent properties, let us hypothesize for the intermediate scattering function a Gaussian behavior with a characteristic relaxation time τ,

$$I(Q, t) = e^{-(t^2/2\tau^2) i^2(Q)}, \qquad (8)$$

results that the resolution effect consists in a partial time integration of the intermediate scattering function, and

$$I(Q, t = 0) \leq S_R(Q, \omega = 0; \Delta\omega) \leq S(Q, \omega = 0). \qquad (9)$$

Figure 1 shows a comparison between $I(Q, t; \tau)$ at a fixed τ value and $R(t; \tau_{\mathrm{RES}})$ for different τ_{RES} values. As pointed out by Fig. 1(a), due to the fact that $\tau \gg \tau_{\mathrm{RES}}$, the only resolution function effect is to select one value of the intermediate scattering function $I(Q, t = 0; \tau)$; by Fig. 1(b) it clearly emerges that the resolution function originates the exclusion of a portion of the intermediate scattering function; in Fig. 1(c) it is shown how, in the measured scattering intensity, the resolution function gives rise to a weighted evaluation of the intermediate scattering function; and, finally, by an inspection of Fig. 1(d), due to the fact that $\tau \ll \tau_{\mathrm{RES}}$, it is evident that there is no effect of the resolution function on the measured scattering intensity, i.e., $S_R(Q, \omega = 0; \Delta\omega) = S(Q, \omega = 0)$.

Let us now consider Eq. (4) and apply the theorem of integral average. We will take into account two cases: (i) τ is longer than τ_{RES} and (ii) τ is smaller than τ_{RES}.

In the first case, we obtain
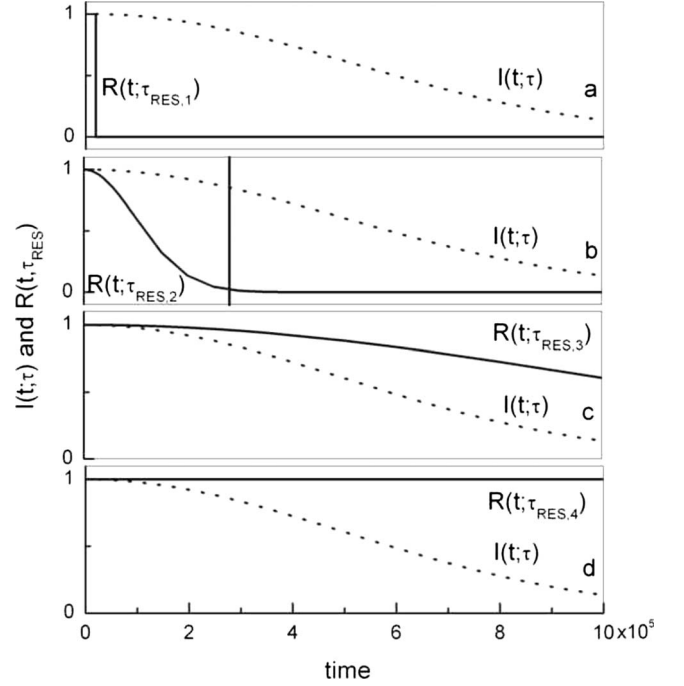
FIG. 1. (a)–(d) Comparison between $I(t; \tau)$, at a fixed τ value and $R(t; \tau_{\mathrm{RES}})$ for different τ_{RES} values.

$$S_R(Q, \omega = 0; \Delta\omega) = \int_{-\infty}^{\infty} I(Q, t) R(t) dt$$

$$= \int_{-\infty}^{-3\tau_{\mathrm{RES}}} + \int_{-3\tau_{\mathrm{RES}}}^{3\tau_{\mathrm{RES}}} + \int_{3\tau_{\mathrm{RES}}}^{\infty}$$

$$\approx \int_{-3\tau_{\mathrm{RES}}}^{3\tau_{\mathrm{RES}}}, \qquad (10)$$

$$S_R(Q, \omega = 0; \Delta\omega) \approx \int_{-3\tau_{\mathrm{RES}}}^{3\tau_{\mathrm{RES}}} I(Q, t) R(t) dt = 6\tau_{\mathrm{RES}} I(Q, t^*) R(t^*), \qquad (11)$$

$$t_{(1)}^* = \pm \sqrt{-2 \frac{\tau^2 \tau_{\mathrm{RES}}^2}{i^2(Q) \tau_{\mathrm{RES}}^2 + \tau^2} \ln\left\{ \frac{\sqrt{2\pi}}{6} \sqrt{\frac{\tau^2}{i^2(Q) \tau_{\mathrm{RES}}^2 + \tau^2}} \right\}}, \qquad (12)$$

and in the second case,

$$S_R(Q, \omega = 0; \Delta\omega) = \int_{-\infty}^{\infty} I(Q, t) R(t) dt$$

$$= \int_{-\infty}^{-3\tau} + \int_{-3\tau}^{3\tau} + \int_{3\tau}^{\infty} \approx \int_{-3\tau}^{3\tau}, \qquad (13)$$

$$S_R(Q, \omega = 0; \Delta\omega) \approx \int_{-3\tau}^{3\tau} I(Q, t) R(t) dt = 6\tau I(Q, t^*) R(t^*), \qquad (14)$$

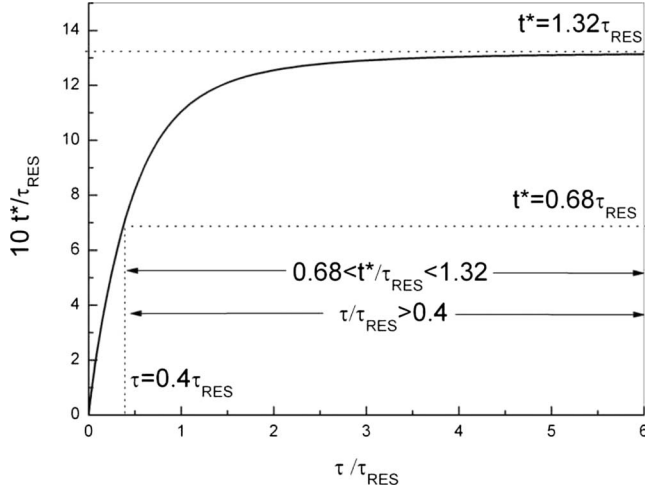FIG. 2. Equivalent time t^* as a function of τ in unit of τ_{RES}.

$$t^*_{(2)} = \pm \sqrt{-2\frac{\tau^2 \tau^2_{RES}}{i^2(Q)\tau^2_{RES}+\tau^2}\ln\left\{\frac{\sqrt{2\pi}}{6}\sqrt{\frac{\tau^2_{RES}}{i^2\tau^2_{RES}+\tau^2}}\right\}},$$
(15)

where t^* is defined as the equivalent time, as it results by the application of the theorem of integral average. Figure 2 shows the equivalent time t^* as a function of the system relaxation time τ; as it can be seen the asymptotic value of t^* at large τ values is $t^*=1.321\tau_{RES}$; in addition for $\tau > 0.4\tau_{RES}$ the equivalent time t^*, with a good approximation, is quite close to τ_{RES}. As a consequence, when the system relaxation time is longer with respect to the time corresponding to the resolution, the scattering function $S_R(Q, \omega = 0; \Delta\omega)$ is proportional to the intermediate scattering function evaluated at the instrumental resolution time, i.e., $I(Q, \tau_{RES})$.

However it should be stressed that it is always possible to find an equivalent time t^*, for which the intermediate scattering function and the measured scattering function are proportional,

$$S_R(Q, \omega = 0; \Delta\omega) \propto I(Q, t^*).$$
(16)

Now, evaluating the spatial Fourier transform of the above equation, one obtains

$$F_r\{S_R(Q, \omega = 0; \Delta\omega)\} \propto G^{self}(r, t^*).$$
(17)

The obtained relationship shows that, due to the fact that the SDF can be normalized, the normalized spatial Fourier Transform (F_r) of the measured EINS intensity profile corresponds to SDF evaluated at t^*. Therefore, a change in the instrumental energy resolution implies a change in the time at which the SDF is evaluated and, hence, a set of SDFs can be obtained by performing EINS measurements at different energy resolutions. The advantage is based on this relationship that has a general character and does not need any restrictive assumption.

IV. ELASTIC INCOHERENT NEUTRON-SCATTERING FUNCTION BEHAVIOR

The intermediate incoherent neutron-scattering function for a system constituted by N particles is well known to be [19,20]

$$I^{inc}(\vec{Q},t) = \frac{1}{N}\sum_i b_i^{inc\ 2}\langle e^{i\vec{Q}\cdot[\vec{r}_i(t)-\vec{r}_i(0)]}\rangle,$$
(18)

where the index i runs over the generic ith scattering particle and b_i is the squared scattering length of the ith particle. Let us operate a partition of the terms contributing to the total intermediate scattering function in groups on the basis of the kind of motion, j, that they can perform

$$I^{inc}(\vec{Q},t) = \frac{1}{N}\sum_j n_j b_j^{inc\ 2}\langle e^{i\vec{Q}\cdot[\vec{r}_j(t)-\vec{r}_j(0)]}\rangle,$$
(19)

in which n_j and b_j^{inc} are the number of j-type groups and the incoherent scattering length of the jth group.

Let us consider, for example, a system in which two groups, indexed A and B, which perform vibrational and vibrational plus rotational motions, respectively, are present. In such a case the intermediate scattering function can be rewritten under the form

$$I^{inc}(\vec{Q},t) = \frac{n_A}{N}b_A^{inc\ 2}\langle e^{i\vec{Q}\cdot[\vec{r}_A(t)-\vec{r}_A(0)]}\rangle + \frac{n_B}{N}b_B^{inc\ 2}\langle e^{i\vec{Q}\cdot[\vec{r}_B(t)-\vec{r}_B(0)]}\rangle$$

$$= \frac{n_A}{N}b_A^{inc\ 2}\langle e^{i\vec{Q}\cdot[\overrightarrow{\Delta r_A^V}(t)]}\rangle + \frac{n_B}{N}b_B^{inc\ 2}\langle e^{i\vec{Q}\cdot[\overrightarrow{\Delta r_B^V}(t)+\overrightarrow{\Delta r_B^R}(t)]}\rangle$$

$$= AI_A^V + BI_B^{V+R},$$
(20)

where I_A and I_B represent the intermediate scattering functions of the two groups and where V and $V+R$ refer to the vibration and to the vibration plus rotation contributions, respectively.

When $\overrightarrow{\Delta r_B^V}(t) \ll \overrightarrow{\Delta r_B^R}(t)$, i.e., when the vibrational displacement can be considered negligible with respect to the rotational one, it results to

$$I^{inc}(\vec{Q},t) = \frac{n_A}{N}b_A^{inc\ 2}\langle e^{i\vec{Q}\cdot[\overrightarrow{\Delta r_A^V}(t)]}\rangle + \frac{n_B}{N}b_B^{inc\ 2}\langle e^{i\vec{Q}\cdot[\overrightarrow{\Delta r_B^R}(t)]}\rangle$$

$$= AI_A^V + BI_B^R.$$
(21)

On the other hand, in a more general case, when the two displacements are quantitatively comparable, under the decoupling approximation, we obtain

$$I^{inc}(\vec{Q},t) = \frac{n_A}{N}b_A^{inc\ 2}\langle e^{i\vec{Q}\cdot[\overrightarrow{\Delta r_A^V}(t)]}\rangle + \frac{n_B}{N}b_B^{inc\ 2}\langle e^{i\vec{Q}\cdot[\overrightarrow{\Delta r_B^V}(t)]}\rangle$$

$$\times \langle e^{i\vec{Q}\cdot[\overrightarrow{\Delta r_B^R}(t)]}\rangle = AI_A^V + BI_B^V I_B^R.$$
(22)

Now considering the single-term contribution and performing a Taylor expansion, we see that an intrinsic deviation from the Gaussian distribution function can be due or to nonzero values of the odd expansion terms, which reflect motion distribution asymmetries, or to even terms higher than the second order that are not referable to the second-order term.
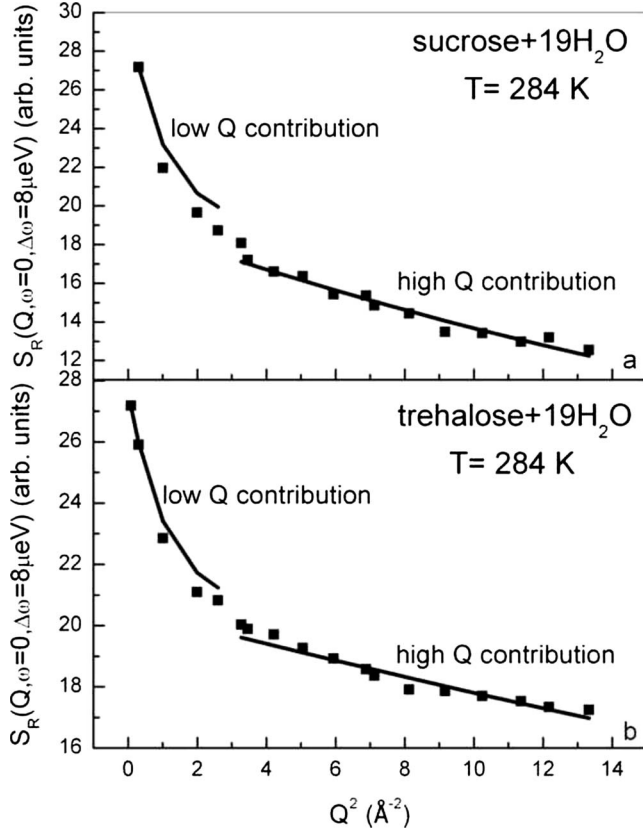
FIG. 3. $S_R(Q, \omega=0; \Delta\omega=8 \ \mu\text{eV})$ for (a) sucrose and (b) trehalose, at $T=284$ K, together with the fit curves of the two partial contributions: one relates to low-Q domain $0-1.7 \ \text{Å}^{-1}$ and the other one to the high-Q domain $1.7-4 \ \text{Å}^{-1}$.

On the other hand, in the presence of two or more processes that are of dynamic heterogeneities, under the hypothesis of a Gaussian behavior for each, one can use a sum of Gaussian contributions, which gives rise to a non-Gaussian behavior, in the analysis of EINS intensity,

$$I^{\text{inc}}(Q,t) = \sum_n \frac{n_n b_n^{\text{inc} \ 2}}{N} e^{-(1/2)Q^2 \langle \Delta r^2 \rangle_n}. \qquad (23)$$

The sum of Gaussian contributions in the analysis of measured EINS intensity profile, besides offering advantages from the formal point of view (e.g., the Gaussian is an eigenfunction of the Fourier transform operator), is widely diffused in literature [25] and successfully employed for fitting experimental data taking into account the limits due to their goodness.

In Figs. 3(a) and 3(b) $S_R(Q, \omega=0; \Delta\omega=8 \ \mu\text{eV})$ and its partial contributions at $T=284$ K for sucrose and trehalose are shown, respectively. As it can be seen the fitting procedure with Eq. (23) provides two contributions which interest more closely two specific Q ranges, i.e., $0-1.7 \ \text{Å}^{-1}$ and $1.7-4 \ \text{Å}^{-1}$. One Gaussian function describes the EINS intensity in the high-Q domain while the other one in the low-Q domain. These two Gaussian functions can be related to different spatial observation windows.
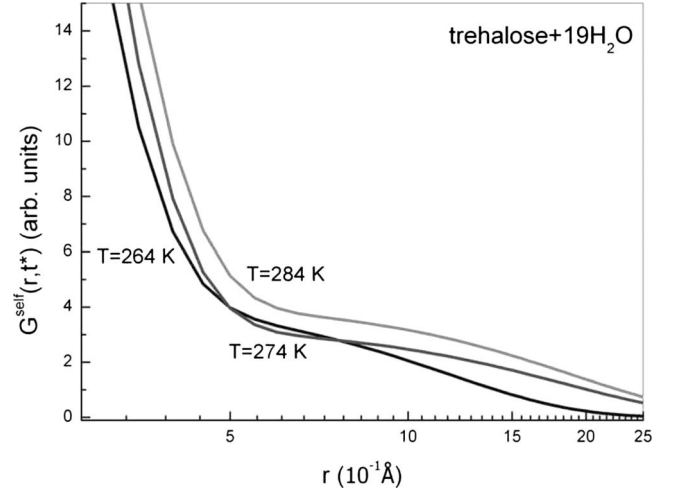

FIG. 4. SDF as a function of r for trehalose at a temperature values of $T=264$, 274, and 284 K.

V. SELF-DISTRIBUTION-FUNCTION PROCEDURE: DISCUSSIONS AND RESULTS

Following Eq. (17) the normalized space Fourier transform of measured EINS intensity profile corresponds to the SDF evaluated at an equivalent time t^*, $G^{\text{self}}(r, t^*)$, which is connected to the instrument resolution energy and to the system characteristic time. In the following, the SDF procedure [5] is revised taking into account the equivalent time. In the framework of the SDF procedure, under the single-process Gaussian ansatz, we obtain

$$G^{\text{self}}(r, t^*) \propto F_r\{S_R(Q, \omega = 0; \Delta\omega)\} = \sum_n A_n F_r\{e^{-Q^2 a_n}\}$$

$$\propto \sum_n A_n G_n^{\text{self}}(r, t^*), \qquad (24)$$

in which $G_n^{\text{self}}(r, t^*)$ are the partial SDFs.

To transform the above proportionality in an identity it is sufficient to normalize the total SDF and the single partial SDFs; this implies that

$$\int_{-\infty}^{\infty} G_n^{\text{self}}(r, t^*) dr = 1 \rightarrow G_n^{\text{self}}(r, t^*) = \frac{1}{2(\pi a_n)^{1/2}} e^{-r^2/4a_n},$$
$$(25)$$

$$A_n \rightarrow B_n = \frac{A_n}{\sum_n A_n}. \qquad (26)$$

Figures 4 and 5 show the obtained SDFs as a function of r for trehalose and dry myoglobin in trehalose, respectively, at different temperature values. In this framework the r^2 mean value results to

$$\langle r^2 \rangle = \int_{-\infty}^{\infty} r^2 G^{\text{self}}(r, t^*) dr = \sum_n B_n \int_{-\infty}^{\infty} r^2 G_n^{\text{self}}(r, t^*) dr$$

$$= 2 \sum_n B_n a_n. \qquad (27)$$

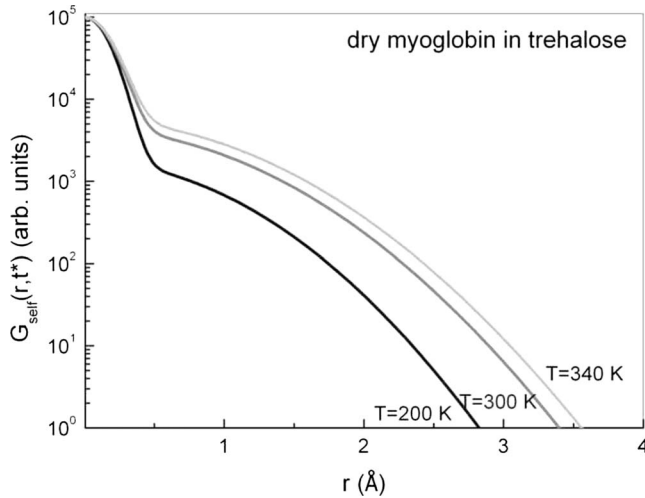FIG. 5. SDF as a function of r for dry myoglobin in trehalose, at the temperature values of $T=178$, 267, and 287 K.

FIG. 6. MSD temperature behavior for trehalose: comparison between Gaussian approximation (different Q-range evaluations) and SDF procedure.

In the following we shall consider the comparison between the Gaussian approximation method and the SDF procedure for the MSD determination. As it is well known, following the former the MSD can be obtained by a linear regression in a Guinier plot of the elastic intensity as a function of Q^2 for a set of points that satisfy the inequality $\vec{Q} \cdot \vec{\Delta r}(t) < 1$, so taking into account the slopes of the measured EINS intensity profile in a Q range starting from $Q = Q_{min}$ up to a given Q' value. Of course at the lowest temperature values, when only a vibrational contribution is present, one can evaluate the intensity profile slope, which is almost constant, in any region of the accessible Q range; this is true also if this contribution decays at $Q > Q_{max}$. In presence of dynamics heterogeneities, starting from a given Q' value and considering smaller and smaller Q' values, the obtained MSD values are dependent on the used Q range.

Now an important point is that the condition $\vec{Q} \cdot \vec{\Delta r}(t) < 1$ when applied for evaluating the intensity limit for $Q = 0$ in the presence of dynamic heterogeneities does not allow us to use all the accessible Q range since it evaluates locally the limit making use of a restricted region of the measured EINS intensity profile.

The SDF can be applied directly to the experimentally determined EINS profiles as well as to whichever function able to reproduce their behavior; it represents an integral procedure which takes into account the global Q behavior and so doing it allows us to reduce the error on the $Q \rightarrow 0$ extrapolation. In addition, the SDF procedure allows us to separate the different MSD contributions.

Figure 6 shows the MSD for hydrated trehalose as obtained by applying the SDF procedure and considering the Gaussian approximation for different Q domains. The results obtained with the SDF procedure, in comparison with the Gaussian procedure, are a more harmonic behavior at low-temperature values, the same dynamical transition temperature, and a more marked dynamical transition.

Now, let us start to observe that, for a given $Q = Q_{max} - Q_{min}$ range, all the motions decaying to zero for $Q > Q_{min}$ contribute to the elastic incoherent scattering intensity; on
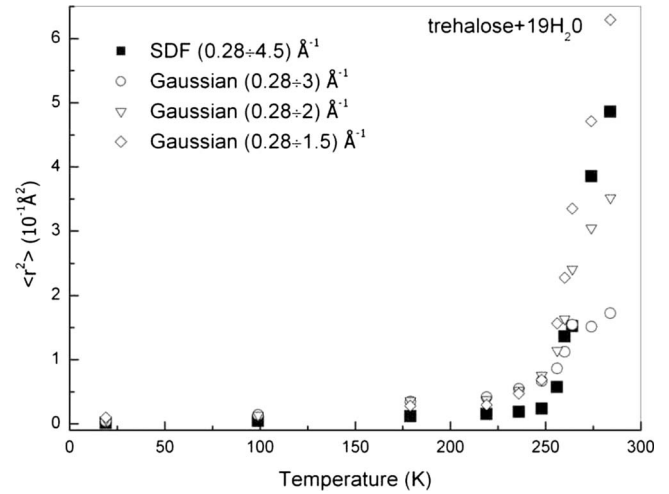
the contrary, the motions whose contribution decays in Q within Q_{min} do not contribute. Figures 7(a) and 7(b) show the obtained SDF and its partial contributions as a function of r at $T=284$ K for sucrose and trehalose, respectively. As it can be seen the different kinds of motion are spatially well separated within the accessible Q range; furthermore, the SDF very closely follows the first partial SDF in the range of $0-0.5$ Å and the second one in the range of $0.5-5$ Å. Analogously, in Fig. 8 the obtained SDF and its partial contributions as a function of r for dry myoglobin in trehalose at $T=200$ K are reported.

By performing the spatial Fourier transform of expression (20) for the intermediate scattering function, one obtains

$$I^{inc}(\vec{Q},t) = A I_A^V + B I_B^{V+R} \rightarrow G^{self}(\vec{r},t) = A G_A^{self,V} + B G_B^{self,V+R},$$

(28)

where the partial SDFs can be associated to the relative scatterer groups. In the case in which the vibrational displacement is negligible respect to the rotational one, the partial
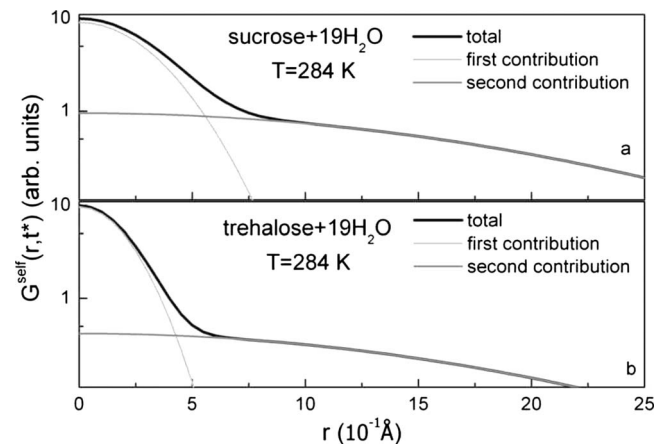

FIG. 7. SDF (black) together their different contributions (gray) for (a) sucrose and (b) trehalose at $T=284$ K.
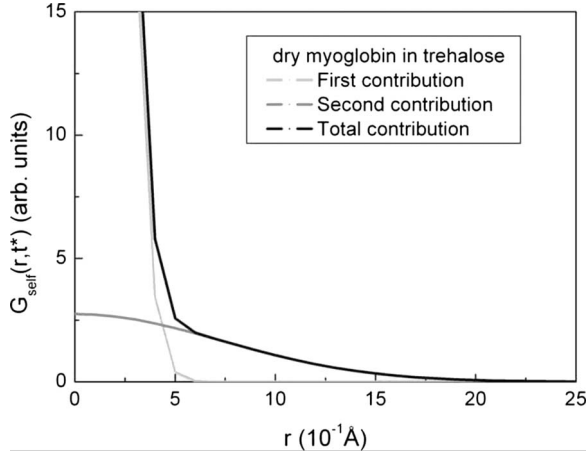
FIG. 8. SDF (black) and its different contributions (gray) for dry myoglobin in trehalose at $T=200$ K.

SDFs can be related to the different kinds of motion, i.e., $A=$vibration and $B=$rotation,

$$I^{\text{inc}}(\vec{Q},t) = AI_A^V + BI_B^R \rightarrow G^{\text{self}}(\vec{r},t) = AG_A^{\text{self},V} + BG_B^{\text{self},R}. \quad (29)$$

On the other hand, in the general case in which the above condition cannot be applied, under a decoupling hypothesis for rotational and vibrational motions, one obtains

$$I^{\text{inc}}(\vec{Q},t) = AI_A^V + BI_B^V I_B^R \rightarrow G^{\text{self}}(\vec{r},t) = AG_A^{\text{self},V} + BG_B^{\text{self},V}$$
$$\otimes G_B^{\text{self},R}. \quad (30)$$

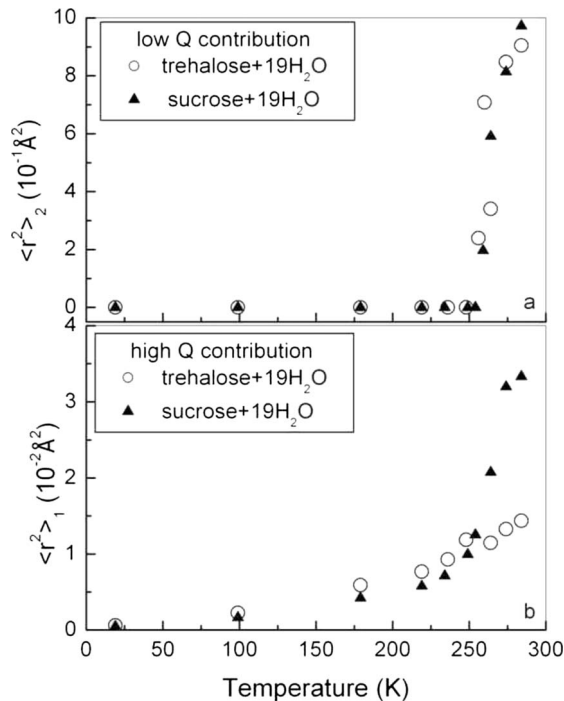It is possible now to obtain the partial MSD values as follows:

FIG. 9. (a) and (b) MSD temperature behavior for trehalose and sucrose spatial observation window analyses.
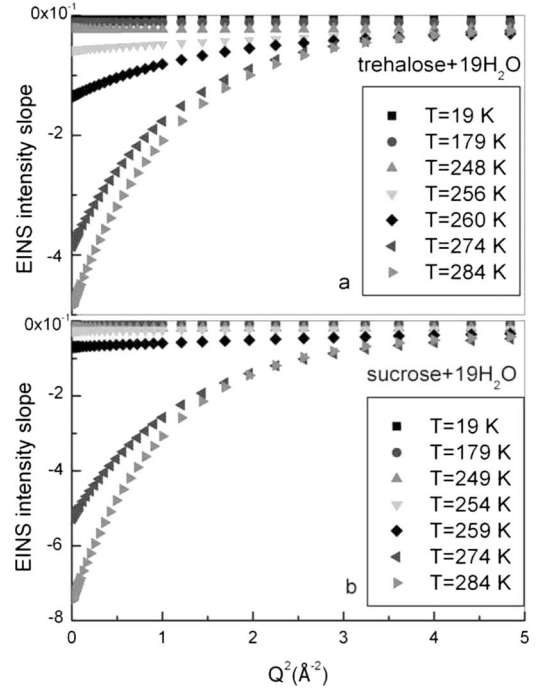

FIG. 10. EINS intensity slopes as a function of Q^2 for trehalose and sucrose.

$$\langle r^2 \rangle_n = \int_{-\infty}^{\infty} r^2 G_n^{\text{self}}(r,t^*)dr = 2a_n. \quad (31)$$

The exponent of each Gaussian is the MSD relative to a particular r domain and the weight A_n is interpretable as the relative percentage weight. Therefore this procedure allows us to obtain the autocorrelation function $G_{\text{self}}(r,t^*)$ versus r, together with its different partial contributions, as well as to determine the partial MSDs, their weights, and the total MSD.

Figures 9(a) and 9(b) show the partial MSDs related for sucrose and trehalose, evaluated by the SDF procedure, in the temperature range of 20–287 K to the high-r domain and to small-r domain, respectively. As it can be seen, the partial MSD behaviors of sucrose and trehalose are equivalent in the high-r domain, whereas they are different in the small-r domain. This circumstance suggests that the higher structure sensitivity of sucrose with respect to trehalose should be related to the small spatial observation windows. It is also important to observe that the dynamical transition temperature of the partial MSDs is equal each other and is equal to the dynamical transition temperature of the average MSD.

Equation (31) can be also expressed by

$$\langle r^2 \rangle = 2\sum_n B_n a_n = \sum_n B_n \langle r^2 \rangle_n. \quad (32)$$

As it can be seen, the MSD is not the simple sum of the different displacement contributions but corresponds to a weighed sum of the MSD contributions associated with the different relaxations in which the weights are obtained by the fitting procedure of measured EINS intensity data.

We can evaluate the MSD by using an alternative way,

$$\langle r^2 \rangle = -2 \left. \frac{\partial I(Q,t)}{\partial Q^2} \right|_{Q=0} = -2 \left. \frac{\partial \sum_n B_n e^{-(1/2)Q^2 \langle \Delta r^2 \rangle_n}}{\partial Q^2} \right|_{Q=0} = -2 \left. \frac{\partial (B_1 e^{-(1/2)Q^2 \langle \Delta r^2 \rangle_1} + \cdots + B_n e^{-(1/2)Q^2 \langle \Delta r^2 \rangle_n})}{\partial Q^2} \right|_{Q=0} \quad (33)$$

$$= \left. \frac{\langle \Delta r^2 \rangle_1 A_1 e^{-(1/2)Q^2 \langle \Delta r^2 \rangle_1} + \cdots + \langle \Delta r^2 \rangle_n A_n e^{-(1/2)Q^2 \langle \Delta r^2 \rangle_n}}{A_1 + \cdots + A_n} \right|_{Q=0} = \frac{\langle \Delta r^2 \rangle_1 A_1 + \cdots + \langle \Delta r^2 \rangle_n A_n}{A_1 + \cdots + A_n}$$

$$= \langle \Delta r^2 \rangle_1 B_1 + \cdots + \langle \Delta r^2 \rangle_n B_n \quad (34)$$

$$= \sum_n B_n \langle \Delta r^2 \rangle_n. \quad (35)$$

Therefore the MSD obtained by SDF procedure represents a good extrapolation to $Q=0$ of the EINS intensity slope. As it can be seen in Fig. 10, by decreasing the Q^2 range the slopes pass from an almost constant value toward a monotonic increase which provide, by their extrapolation to zero, the half of the MSD.

VI. CONCLUSIONS

In the present paper the evaluation of the resolution effect on the measured EINS intensity profile is considered. It is shown that the resolution effect consists in the partial time integration of the intermediate scattering function. We considered two limit cases: (i) when $\tau \ll \tau_{\text{RES}}$, one obtains $S_R(Q, \omega=0; \Delta\omega) = S(Q, \omega=0)$ and (ii) when $\tau \gg \tau_{\text{RES}}$, one gets $S_R(Q, \omega=0; \Delta\omega) = I(Q, t=0)$. We have also defined an equivalent time t^*, for which the normalized spatial Fourier transform of the measured EINS intensity profile corresponds to the SDF evaluated at $t=t^*$. In the case for which $\tau \gtrsim 0.4\tau_{\text{RES}}$ it results to $t^* \approx \tau_{\text{RES}}$. On this concern, starting

from the general form of the intermediate incoherent scattering function, it is possible to introduce a fitting expression for measured EINS intensity profile containing the average displacements associated with the different spatial domains together with their relative weights. A comparison between the SDF and the Gaussian procedure is presented.

By applying the SDF procedure to water-homologous disaccharide mixtures, a different dynamical behavior in the large-Q range region is pointed out at temperature values higher than about 250 K. It emerges that the hydrogen bond imposed network of the water-trehalose mixture appears to be stronger with respect to that of the water-sucrose mixture and this result can justify the highest bioprotectant effectiveness of trehalose in comparison with sucrose.

[1] B. Alefeld, A. Kollmar, and B. A. Dasannachrya, J. Chem. Phys. **63**, 4415 (1975).

[2] W. Doster, M. Diehl, R. Gebhardt, R. E. Lechner, and J. Pieper, Chem. Phys. **292**, 487 (2003).

[3] M. Diehl, W. Doster, W. Petry, and H. Schober, Biophys. J. **73**, 2726 (1997).

[4] W. Doster, M. Diehl, W. Petry, and M. Ferrand, Physica B **301**, 65 (2001).

[5] S. Magazù, G. Maisano, F. Migliardo, and A. Benedetto, Phys. Rev. E **77**, 061802 (2008).

[6] S. Magazù, Physica B **226**, 92 (1996).

[7] F. Affouard, P. Bordat, M. Descamps, A. Lerbret, S. Magazù, F. Migliardo, A. J. Ramirez-Cuesta, and M. F. T. Telling, Chem. Phys. **317**, 258 (2005).

[8] S. Magazù, F. Migliardo, and A. J. Ramirez-Cuesta, J. R. Soc., Interface **2**, 527 (2005).

[9] S. Magazù, F. Migliardo, and M. F. T. Telling, J. Phys. Chem. B **110**, 1020 (2006).

[10] S. Magazù, F. Migliardo, and M. T. F. Telling, Food Chem.

106, 1469 (2008).

[11] J. C. Kendrew, R. E. Dickerson, B. E. Strandberg, R. G. Hart, D. R. Davies, D. C. Phillips, and V. C. Shore, Nature (London) **185**, 422 (1960).

[12] S. Cusack and W. Doster, Biophys. J. **58**, 243 (1990).

[13] R. J. Loncharich and B. R. Brooks, J. Mol. Biol. **215**, 439 (1990).

[14] J. Smith, K. Kuczera, and M. Karplus, Proc. Natl. Acad. Sci. U.S.A. **87**, 1601 (1990).

[15] J. S. Ahn, Y. Kanematsu, M. Enomoto, and T. Kushida, Chem. Phys. Lett. **215**, 336 (1993).

[16] E. R. Henry, W. R. Eaton, and R. M. Hochstrasser, Proc. Natl. Acad. Sci. U.S.A. **83**, 8982 (1986).

[17] L. Cordone, M. Ferrand, E. Vitrano, and G. Zaccai, Biophys. J. **76**, 1043 (1999).

[18] G. Cottone, L. Cordone, and G. Cicciotti, Biophys. J. **80**, 931 (2001).

[19] M. Bee, *Quasielastic Neutron Scattering* (Hilger, Bristol, 1988).

[20] F. Volino, *Spectroscopic Methods for the Study of Local Dynamics in Polyatomic Fluids*, NATO ASI-Series B, edited by J. Dupuy and A. J. Dianoux(Plenum, New York, 1978), Vol. 33.

[21] L. Van Hove, Phys. Rev. **95**, 249 (1954).

[22] W. Doster, S. Cusak, and W. Petry, Nature (London) **337**, 754 (1989).

[23] W. Doster and M. Settles, in *Hydration Processes in Biology: theretical and Experimental Approaches, NATO Advanced Studies Institute, Series A: Life Sciences*, edited by M. C. Bellissent-Funel and J. Teixera (IOS, Amsterdam, 1998), Vol. 305, p. 177.

[24] W. Doster and M. Settles, Biochim. Biophys. Acta **1749**, 173 (2005).

[25] T. Becker and J. C. Smith, Phys. Rev. E **67**, 021904 (2003).